Fluorescence signals of core–shell quantum dots enhanced by single crystalline gold caps on silicon nanowires

2009 Nanotechnology 20 165301

(http://iopscience.iop.org/0957-4484/20/16/165301)

Nanotechnology **20** (2009) 165301 (9pp) doi:10.1088/0957-4484/20/16/165301

Fluorescence signals of core–shell quantum dots enhanced by single crystalline gold caps on silicon nanowires

S H Christiansen[1,2], J W Chou[1,3], M Becker[1,2], V Sivakov[1,2], K Ehrhold[1], A Berger[1,2], W C Chou[3], D S Chuu[3] and U Gösele[1]

[1] Max-Planck-Institute of Microstructure Physics, Weinberg 2, D-06120 Halle, Germany
[2] Institute of Photonic Technology (IPHT), Albert-Einstein-Strasse 9, D-07745 Jena, Germany
[3] Department of Electrophysics, National Chiao Tung University, Hsingchu 30050, Taiwan

Received 6 September 2008, in final form 13 February 2009
Published 31 March 2009
Online at stacks.iop.org/Nano/20/165301

Abstract
We use nanoscale (20–300 nm in diameter) single crystalline gold (Au)-caps on silicon nanowires (NWs) grown by the vapor–liquid–solid (VLS) growth mechanism to enhance the fluorescence photoluminescence (PL) signals of highly dilute core/shell CdSeTe/ZnS quantum dots (QDs) in aqueous solution (10^{-5} M). For NWs without Au-caps, as they appear, for example, after Au etching in aqua regia or buffered KI/I_2-solution, essentially no fluorescence signal of the same diluted QDs could be observed. Fluorescence PL signals were measured using excitation with a laser wavelength of 633 nm. The signal enhancement by single crystalline, nanoscale Au-caps is discussed and interpreted based on finite element modeling (FEM).

1. Introduction

Semiconductor quantum dots (QDs) have optical and electronic properties which are strongly dependent on the QD size, due to quantum confinement of the charge carriers involved [1, 2]. For two decades now, extensive research has been carried out to define and explore QD applications in optoelectronics and memory devices [3–5]. Only 10 years ago, were Alivisatos *et al* able to present a recipe to make QDs water soluble so that QDs could thus be combined with biological molecules [6, 7], a finding that opened up additional options to integrate QDs in biological and medical studies. One of the important features of QDs is that the particle size determines many of the QD properties, such as the wavelength of the fluorescence emission. By altering the QD size and its chemical composition, fluorescence emission may be tuned in a broad wavelength range of 400–2000 nm [8–12]. Given that fact, the utilization of QDs as fluorescent labels for biological macromolecules has attracted considerable attention. The current methods of producing QDs by chemical synthesis allow for excellent control over the mean particle size and particle size distribution, allowing milligram or gram quantities of QDs where the particles exhibit narrow and symmetric emission peaks (full width at half maximum (FWHM) typically in the few tens of nanometers range). This is much better than the emission characteristics for typical organic dye molecules, which often have much broader and asymmetric emission profiles. This particular property of QDs is useful when simultaneous labeling and detection of multiple analytes is desired [13]. In addition to their controllable photon emission properties, QDs show advantageous absorption properties. Unlike organic dyes, which show large absorption cross-sections only across a narrow band of resonant frequencies, the relatively large densities of states and overlapping band structures in semiconductor materials result in QDs with high molar absorption capabilities and broad absorption spectra [14]. This property allows efficient excitation of multiple QD-based fluorophores with a single light source. The combination of large molar absorption capabilities and high quantum yield provides the basis for a series of QD-based fluorescent labels. In fact, studies comparing the brightness of single CdSe/ZnS core/shell QDs to that of single rhodamine 6G molecules indicate that the fluorescent photon flux in QDs is 10–100-fold larger [7]. Several other QD properties have significant practical implications for their use as fluorescent labels. For example, their low photo-degradation rates make continuous or long-term monitoring of slow biological processes possible (very challenging for traditional organic fluorophores) [7, 15]. The long fluorescence lifetimes of QDs, on the order of 10–50 ns, are advantageous

for distinguishing QD signals from background fluorescence and for achieving high-sensitivity detection [6]. QD labels have successfully been used, as a replacement for organic dyes, for a variety of bio-analytical purposes, such as DNA hybridization detection [16, 17], immunoassays [18], and binding assays using fluorescence resonant energy transfer (FRET) to probe for target events [19–24]. In the area of biosensors, QDs are used for their long-term photostability, allowing real-time and continuous monitoring.

In this study we use commercial core/shell CdSeTe/ZnS colloidal QDs in a dilute aqueous solution (10^{-5} M) that show fluorescence photoluminescence (PL) in a narrow energy range. We show that we are able to enhance the PL signal intensity by a factor larger than 100 by bringing the QDs in close vicinity to gold (Au)-caps which reside atop silicon nanowires when grown Au-catalyzed following the vapor–liquid–solid (VLS) growth mechanism [25, 26] from the gas phase by evaporating silicon from a solid target using an electron beam [27, 28]. The PL signal enhancement is mediated by the electrical field enhancement at the nanoscale Au-caps. This optical near-field phenomenon is discussed based on two-dimensional (2D) finite element modeling (FEM) as are the implications for applications in the aforementioned fields.

2. Experimental details

We are interested in a PL study of QDs of a commercially available core/shell type, CdSeTe/ZnS [30], with 5.3 nm diameter at the low concentration of 10^{-5} M in aqueous solution. For the PL studies, different substrates were spin-coated with the QD suspension at ∼5000 rpm for several minutes. That way we expect to have well-separated single QDs on the different substrate surfaces.

The PL measurements were carried out in a Jobin Yvon LabRam HR800 spectrometer using a He–Ne laser (wavelength 633 nm) for exciting fluorescence of the QDs. An objective with 100× magnification (numerical aperture: 0.9) was used. The laser power was reduced with a density filter down to ∼3 mW. The entrance filter was used to filter out background light from the spectrum and a notch filter was used to remove the exciting laser light from the spectrum.

The time-correlated single photon counting (TCSPC) measurements for single QDs sitting on silicon nanowires (SiNWs) with and without Au-caps were carried out by using laser excitation by a picosecond pulsed diode laser with a repetition frequency of 10 MHz operating at a wavelength of 405 nm, a power ∼0.13 μW, and a pulse width of 50 ps. The single QD excitation can be realized by directing the laser onto the sample by an optical fiber. After the excitation (of the order of ∼ns), the electron–hole pair that is excited recombines and emits a photon (fluorescence) that can be detected. The fluorescence signal goes through a long pass (500 nm) filter, and then passes through a pin hole (50 μm) and is expanded by two lenses. Finally, the expanded fluorescence goes through a filter again and is then focused onto a single photon avalanche photodiode (SPAD; the response time is about 400 ps) which turns the light signal into an electrical signal for time-tagged time-resolved (TTTR) analysis. With this experiment we study and compare the TCSPC measurements of single QDs on SiNWs with and without Au-caps.

The SiNWs were grown by the Au-catalyzed vapor–liquid–solid (VLS) growth mechanism [25, 26], making use of the incorporation of silicon atoms in the epitaxially (with respect to the Si(111)-wafer substrate) growing SiNWs, evaporated by an electron beam (EBE, electron beam evaporation) [27, 28]. The silicon substrate pieces were cleaned by rinsing in acetone for 5 min followed by an ethanol rinse for another 5 min prior to nanowire growth. Native silicon dioxide layers were removed by etching with 40% HF for 30 s followed by a 2% HF rinse for 3 min. Finally, the samples were rinsed with de-ionized water and were blow dried with nitrogen. This cleaning procedure yields hydrogen-terminated silicon surfaces (for a limited time of a few minutes), which allowed for subsequent deposition on an essentially oxide-free surface. Initially, a 2.4 nm thick Au film was sputtered (EDWARDS, Sputter Coater S150 B) on the cleaned, oxide-free wafers to create a continuous Au layer which disintegrates upon heating (above the eutectic temperature of Au–Si of 370 °C) into Au-caps that catalyze straight SiNW growth on the Si(111) substrate wafer perpendicular to the sample surface. Then samples were heated for 30 min to temperatures of 650 °C in the evacuated growth chamber (base pressure 2–5 × 10^{-7} Torr) to produce growth templates that consist of Au-nanocaps on the oxide-free Si substrates. The EBE system used for SiNW growth in this work was built in house. The silicon is evaporated from a water cooled copper crucible using an electron beam at a beam current of 35–80 mA. The higher the evaporation current, the larger the growth velocities of the SiNWs [27]. All growth experiments were carried out for 10 min and 1 h at 650 °C and at a chamber pressure of 2–5 × 10^{-7} Torr and an evaporation current of 80 mA. The growth rates of SiNWs under these conditions were in the region of at most 100 nm min^{-1} (achieved essentially on the virgin substrate at the beginning of the growth process) [28].

SiNWs and QDs were analyzed using scanning electron microscopy (SEM) in a conventional Jeol 6300F and a high resolution FEI Nova Nanolab 600 with in-lens detector that permits highest resolution of 1 nm at 15 kV and 5 mm working distance and still 2 nm at low voltages down to 1 kV at 1.5 mm working distance, i.e. sufficiently good to distinguish the 5.3 nm QDs. The SiNWs were moreover characterized by transmission electron microscopy (TEM) in an FEI CM200UT.

Finite element calculations [31] were carried out using the COMSOL software (www.femlab.de). The classical Maxwell's equation system, especially the Helmholtz wave equation, was solved with thin film experimental data of Johnson and Christie [29] as an input for the dielectric material's response. This approach allows us to delineate comparably realistically the geometrical appearance of our SiNWs. However, our simulations are 2D (to reduce solving times at the required fine meshing in structures as complex as our SiNWs) whereas the SiNWs are 3D features and we truly underestimate the achievable field enhancement when using 2D instead of 3D simulations [40]. Therefore, we may consider our simulations as a lower limit of what is in principle achievable in terms of field enhancement.

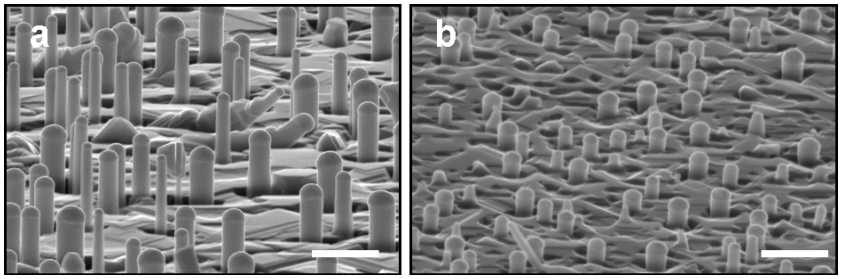

Figure 1. SEM images of Si NWs grown by EBE at 650 °C: (a) 1 h; (b)10 min. The scale bar for (a) and (b) is 1 μm.

Our SiNW geometry is given by 200 nm wide and 400 nm long SiNWs on a Si substrate with a Au-cap that is either truly hemispherical or slightly faceted. The active domain for the calculation is 2×2 μm^2. We tested the convergence of our models for different mesh sizes via the evaluation of the normalized electric field at the center of the gold hemisphere and found the applied mesh to be sufficiently fine to not obtain mesh-dependent results. We chose an adaptive meshing with a maximum grid size of 1 nm at all surfaces. So we ended up with a relatively coarse mesh within the silicon NW shaft of 50 nm but a very fine one in the sensitive surface regions of the Au-cap, thus realizing an optimum compromise between exactness and solving time. The incident electric field is assumed as an electromagnetic plane wave with in-plane polarization (TM mode). As a variable parameter we chose the wavelength of the incident laser light, varying from 220 to 900 nm in 2 nm steps.

The single crystallinity of the Au-caps was verified by electron back-scatter diffraction (EBSD) in a scanning electron microscope (TESCAN, LYRA equipped with an AMETEK, TSL EBSD system).

3. Results

We will show that we can enhance the fluorescence photoluminescence (PL) signal of the QDs by Au nanoparticles (named caps throughout the paper) as they form on SiNWs that were grown by the vapor–liquid–solid (VLS) growth process. The enhancement constitutes an optical near-field effect that will be described and discussed in the following, supported by finite element modeling (FEM) using the COMSOL code.

Typical SiNWs grown by EBE are shown in figure 1(a) (1 h growth) and (b) (10 min growth). The difference in the samples is the growth time of SiNWs. Statistical data of NW lengths and diameters are taken from SEM investigations. The SiNW statistics give the following lengths and diameter values: after 10 min the SiNWs are 350 ± 50 nm long and 200 ± 30 nm in diameter; after 1 h the SiNWs are 650 ± 100 nm long and 325 ± 80 nm in diameter. For 10 min growth the effect of surface migration of Au atoms over the surface is less pronounced [32–34]. This explains the reason the NWs are of relatively identical lengths independent of the Au-cap diameter. After 1 h growth, Ostwald ripening effects [32–35] are discernible (figure 1(b)) in the sense that bigger Au-caps grow bigger and smaller caps shrink further. Concomitantly, the smaller the cap the thinner the SiNW, and thus the faster the growth, since less material needs to be incorporated into the growing SiNW shaft. As a result, thinner SiNWs (e.g. $<$100 nm in diameter) grow faster, and after 1 h growth time they are already substantially longer than thicker (e.g. $>$300 nm) ones (see figure 1(b)).

As concerns the size of the Au-caps, we have a distribution of cap diameters in both samples, with a stronger scatter due to the Ostwald ripening after longer growth times. On average, however, the diameters for both samples lie between $\sim$200 and 300 nm. The Au-caps assume in any case a close to half-spherical shape, often with some facets, and are all single crystalline [36].

For some samples, the Au-caps atop the Si NWs and on the SiNW shaft surfaces were removed by exposing them to aqua regia or an aqueous solution of KI/I_2 (4:1) for 15 min (which are both known to be effective Au etchants) [37] after Au agglomeration on the surfaces by annealing at 800 °C for 20 min in air and subsequent oxide removal by a HF dip (hydrofluoric acid; 4% HF in H_2O-dest (distilled water), for 10 min). An SEM analysis showed that the big Au-caps atop an NW and the smaller caps or Au clusters on the SiNW shaft surfaces were entirely removed after the treatment. In SEM we do not see any sign of remaining Au particles on the surface that give rise to strong scattering, so that they are usually easily discernible in a secondary electron image as bright spots. In TEM studies we revealed that only on very rare occasions (one of these is selected for the TEM image in figure 2; the Au particle is indicated by an arrow) very small (a few nanometers in diameter) Au agglomerates still remain. They are most probably composed of a Au–Si alloy, so they are not as easily attacked by the gold-removing chemistry.

PL measurements were carried out for CdSeTe/ZnS QDs residing on a (i) bare Si(111) wafer, (ii) a Si(111) wafer with EBE SiNWs after 10 min and (iii) 1 h of growth, and (iv) a Si(111) wafer with SiNWs after 1 h of growth after Au removal in KI/I_2 etchant. For direct comparison, PL measurements of the bare Si(111) wafer and the substrate wafer with SiNWs (1 h of growth) without any QDs were carried out.

All results of the PL study are shown in figure 3. No pronounced PL signal is visible for QDs on the substrate wafer alone (red line). No PL signal is visible for substrates without QDs, i.e. the bare substrate, nor for the bare substrate with SiNWs where the Au-caps have been removed (black line). However, an increased PL signal was found for all SiNWs (for both growth times) with Au-caps atop (green and turquoise line).

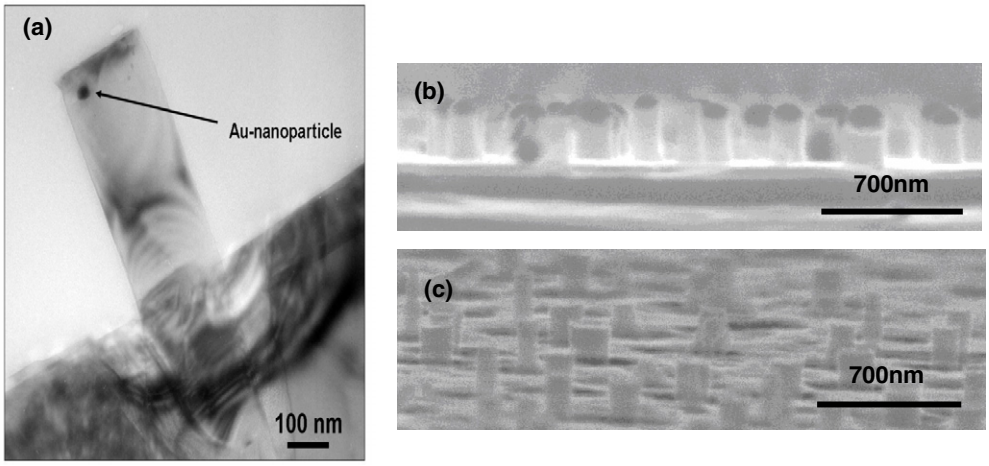

Figure 2. (a) TEM cross-sectional micrograph of a Si NW grown by EBE at 650 °C for 1 h from a Au-cap as the catalyst for the VLS growth. The Au on the SiNW surface agglomerated on the SiNW shaft by annealing the sample at 800 °C for 20 min in air. The Au-caps and agglomerates were removed by etching the sample in an aqueous solution of KI/I_2 (4:1) for 10 min after the surface SiO_2 that formed during oxidation had been removed by a HF dip (4% HF in H_2O-dest, for 10 min). As a result, the SiNW remained without the Au-cap atop and is essentially a shaft that is free of Au agglomerates. On very rare occasions (we found this one example in an analyzed area of TEM samples of $\sim 5\ \mu m^2$) there remain Au agglomerates on the wire shaft that are not removed by the chemical treatment (indicated by an arrow here). These may consist of a Au–Si alloy that is resistant against the etch; (b) cross-sectional SEM micrograph of SiNWs from figure 1(a); (c) oblique SEM micrograph of SiNWs from (b) after chemical Au-cap removal.

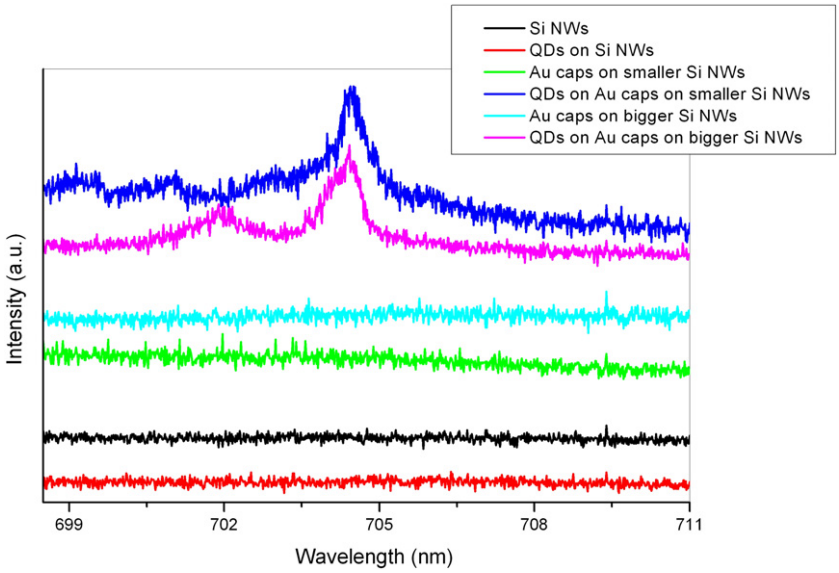

Figure 3. Fluorescence PL study of core/shell CdSeTe/ZnS QDs on different substrates, including SiNWs with nanoscale Au-caps (blue and magenta lines). QDs are luminescent only when residing close to a Au-cap. QDs at the present dilution do not luminesce when residing on bare silicon surfaces (polished substrate surface or rough surface on the nanoscale due to SiNWs without the catalyzing Au-cap: red curve) nor do the bare surfaces luminesce without QDs (black, light blue, green curves).

A pronounced PL signal with peaks at the QD emission range is only visible at this dilute concentration of QDs on the substrate surface when the QDs are in close vicinity to a nanoscale Au-cap. PL signals of QDs on Au-caps are indicated by the blue and magenta lines. The characteristic fluorescence signal of the core/shell QDs is visible. The difference in the fluorescence signal of the QDs on the different SiNW samples can be interpreted as being a result of different size and composition of the QDs within the measured spot. Even though the QDs were purchased as a commercial product, the vendor does still allow a fluctuation in size and composition to a small extent that, however, may be enough to account for the PL signal differences. Another finding is that different PL signals were measured on different areas of the sample.

In figure 4 we see no PL fluorescence signal of the QDs at an area where no SiNW was observed (black circle). We observe a pronounced PL signal (green line) that is very similar to the blue line signal in figure 3 when QDs reside directly on the Au-cap of SiNWs (1 h of growth). We observe a faint PL fluorescence which is, however, more than just background

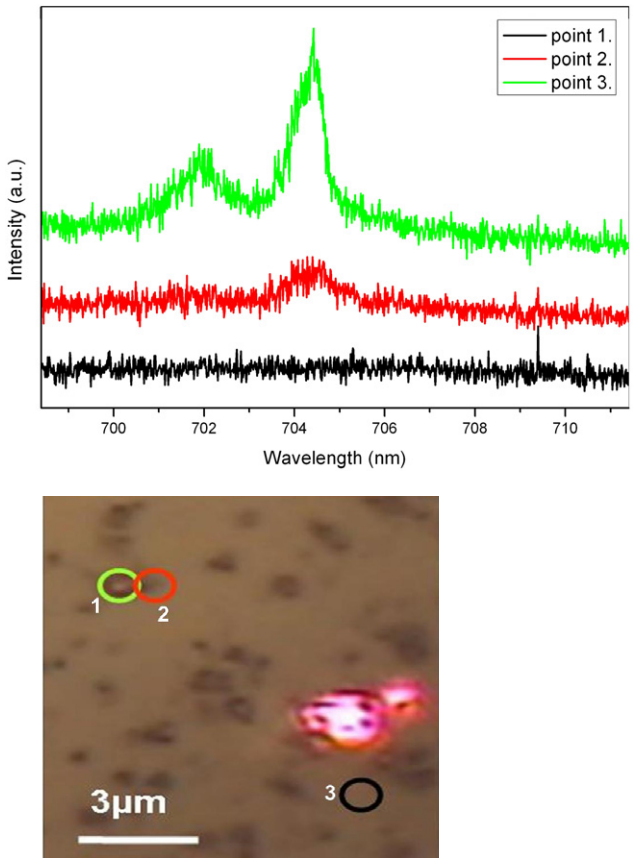

Figure 4. Fluorescence PL measurements of core/shell CdSeTe/ZnS QDs on SiNWs with nanoscale Au-caps on Si(111) substrates as they form by the Au-catalyzed VLS EBE growth. Single QD luminescence is discernible strongly enough only when residing on a Au-cap (green line). Single QDs on the bare Si(111) surface do not give rise to a characteristic QD fluorescence PL signal (black line). The PL signal of ensembles of QDs may faintly appear if enough of them are close together as they are sometimes close to a SiNW (see figure 5, top row, right) (red line). The reddish spot is due to reflected light of the focused laser on the sample surface.

noise when measuring not exactly on the Au-cap but close to it on the substrate surface (figure 4, red line). These findings can be interpreted based on a SEM study of the QD distribution after the spin coating procedure on the smaller SiNW sample surfaces. Using the high resolution SEM of a dual beam FIB system (NOVALAB, FEI) with in-lens detector it is possible to resolve the QDs on the sample surface. We find that well-separated QDs are spread over the sample surface and reside somewhere on the crystallographically faceted substrate surface or rarely on the Au-caps of the SiNWs too. On rare occasions even more than one QD resides on the Au-cap of a SiNW. It appears that the distribution of QDs is not exactly random. Close to the Au-caps with QDs, the QD density on the sample surface is usually higher too. On the other hand, there are areas that do not contain any QD whatsoever, neither on the NWs nor on the sample surface. This observation supports the PL results of figure 4 that suggest that single QDs on bare Si substrates do not give rise to the characteristic QD PL signal, but that QDs at higher density may give rise to a faint noisy QD PL and that even single QDs on Au-caps give rise to a more pronounced PL signal.

4. Discussion

The PL fluorescence signal enhancement by single crystalline Au-caps on VLS SiNWs can be interpreted in terms of enhancement effects that can reach several orders of magnitude depending strongly on the morphology and shape of the metal (here Au) nanofeatures (here hemispherical, sometimes slightly faceted Au-caps) as well as their crystalline nature. The single crystalline nature of Au-caps favors maximum possible enhancement for otherwise given boundary conditions due to the fact that no lattice defects disturbing single crystallinity give rise to plasmon scattering. Figure 6 gives a proof of the single crystallinity of the Au-caps. An EBSD pattern is shown that is superimposed on a SEM micrograph of a SiNW. The color code shows that the orientation of the Au-cap is not in registry with the SiNW [111]-direction. The orientation can be deduced from the color code. The fact that a single color appears is proof of single crystallinity. Larger statistics given by several EBSD patterns of different SiNW Au-caps show that the orientation of the caps differ but that all caps are single crystalline for the growth conditions used (for more details of this analysis see [46]).

The reason for the strong PL signal enhancement is still subject to some controversy [38, 39]. Two different mechanisms seem to be involved. The so-called pure electromagnetic effect is due to plasmon resonances of the metal nanoparticles. The electromagnetic near field of a metal particle within this model can exceed the applied field by orders of magnitude. An additional enhancement can be caused by charge transfer or bond formation between the sample and the metallic substrate, which can strongly enhance the polarizability of, for example, a molecule. The electromagnetic near-field enhancement of a metal nanoparticle can affect the PL fluorescence of our QDs. Typical near-field enhancement factors as calculated by the finite element method [31] can reach values of 3–5, strongly depending on the geometry of the metal nanoparticle and the metal particle orientation with respect to the incident laser light. Let us again mention that our models are 2D, and therefore the estimated enhancement factors give a lower limit of the electromagnetic enhancement to be expected. (This is due to the fact that spheres show stronger resonances than infinitely long cylinders which we had implicitly assumed.) Examples of the electromagnetic near-field enhancement are given in the 2D FEM micrograph in figure 6, where the SiNW with Au-cap atop is shown as well as the polarization of the incident laser light for the example of incident laser light to be under 45° to the SiNW axis (polarization of the laser light parallel to SiNW axis is denoted 0°). The SiNW in our example has a diameter of 200 nm and a length of 400 nm, and the Au-cap is hemispherical (left) and (111) and (110) faceted (right). The color code indicates the dimensionless enhancement factor which is given by the absolute value of the local time averaged electric field normalized by the incident field.

The maximum enhancement achievable with 633 nm excitation wavelength and incidence of the polarized laser light under 45° with the type of Au-caps on VLS SiNWs we have is given by the hemispherical cap with an enhancement factor

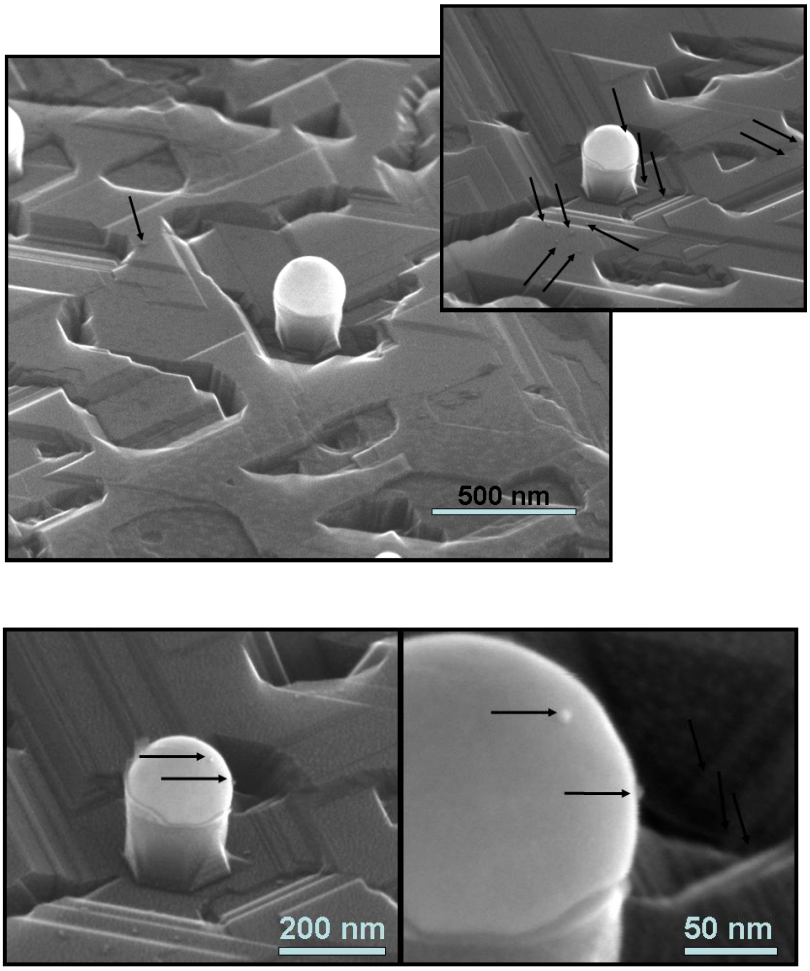

Figure 5. High resolution SEM micrographs that show the ∼5 nm core/shell CdSeTe/ZnS QDs on SiNWs with nanoscale Au-caps on Si(111) substrates as they form by the Au-catalyzed VLS EBE growth. QDs in the top row of micrographs are very rare in the left picture and they occur at higher density in the right picture, which was taken at another spot on the sample. At areas where QDs reside on the Au-caps they are usually also found at higher density, especially at the facets of the substrate surface. The bottom row of micrographs show an enlargement of the QDs at the Au-cap surface. From these pictures the ∼5 nm diameter of the QDs is clearly discernible.

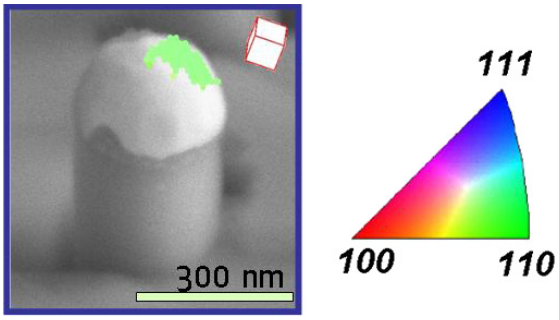

Figure 6. Electron back-scatter diffraction pattern of a Au-cap on a SiNW. Due to the 3D geometry of the SiNW, shadowing effects occur during EBSD. That is why EBSD allows mapping of only part of the Au-cap. However, this part that can be mapped is single crystalline, as is seen from the entirely undisturbed green color. The same single crystallinity holds for all the Au-caps on VLS SiNWs that have been investigated (the number is >8).

of 3.6, according to the 2D FE simulations in figure 6, which leads to an intensity of 3.6^2. The fluorescence field at 704 nm (i.e. where the QDs have their resonances according to figures 3 and 4) shows a factor of 3.3 (according to 2D FE simulations as shown in figure 8), which leads to an intensity of 3.3^2. The overall maximum enhancement can thus be $3.6^2 \times 3.3^2$, i.e. ∼140.

The enhancement factor at the QD resonance of 704 nm can be deduced from 2D FE simulations in figure 8 where the enhancement factor depending on excitation wavelength is plotted for the geometrical point on the Au-cap surface of maximum enhancement. Figure 8 shows a rather complex sequence of resonances depending on wavelength for the rather complex geometry of a slightly faceted or totally roundish Au-cap (both can experimentally be realized and controlled) sitting on pronounced SiNW shafts. The resonance at 704 nm coincides with an enhancement factor of 3.3.

A definite interpretation of the mechanism of the PL enhancement requires further experiments. However, some points for discussion of PL enhancement can be given. First of all, the illumination was kept constant for all experiments, with and without Au-caps being present for the PL measurements of QDs. Therefore, the enhancement of PL intensity of QDs when Au-caps are present most probably follows the mechanism

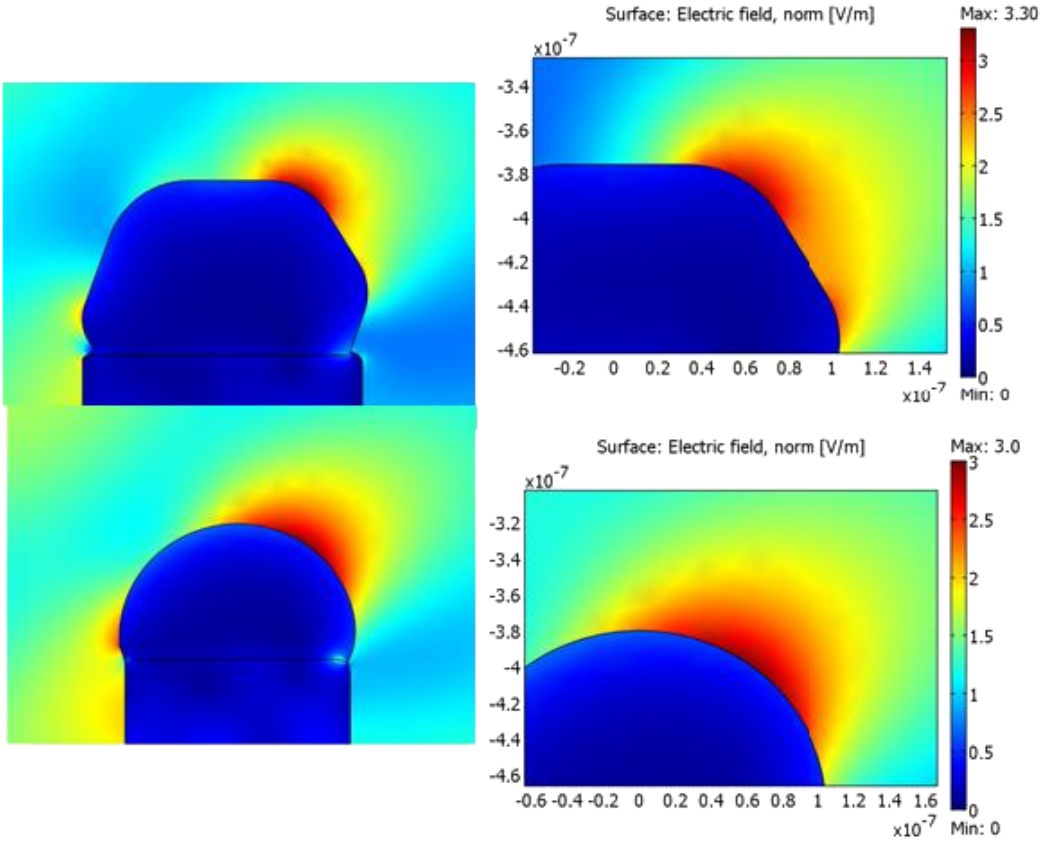

Figure 7. Finite element modeling of the electromagnetic field enhancement at a SiNW with Au-cap atop. The color codes indicate the field enhancement factor as given by the local field divided by the incident field; light incident under 45°, 633 nm laser wavelength; (left) hemispherical cap, (right) (111) and (110) faceted cap.

that was suggested before for dye molecules combined with silver nanoparticles by Kalele *et al* [41]. This mechanism of increased PL in the vicinity of coinage metal nanoparticles is based on a higher excitation of the QD (higher absorption) there. The exciting light has a higher electric field strength close to the metal nanoparticles, here the Au-caps, and this then indirectly corresponds to a higher flux of photons and a higher probability of exciting the QDs. This in turn leads to a higher PL intensity. The opposite case, that PL quenching occurs in close vicinity to metal nanoparticles, is not observed in our case, and is therefore not discussed any further. Our observation, however, coincides with the earlier observation that when metal nanoparticles are in close proximity to fluorophores, for example, quenching of luminescence occurs, whereas when metal nanoparticles are located at a certain distance, enhancement in luminescence is observed. This effect has been explained by the coupling of surface plasmon resonances from metal nanoparticles with the fluorophores, resulting in an increase of the excitation and emission rate of the fluorophore in the localized electromagnetic field [41–43]. The quenching and enhancement of luminescence intensity of the dye molecules was alternatively also explained as the transfer of electrons from the dye to the silver nanoparticles. Partly, this was also attributed to the aggregation of dye molecules upon addition of silver nanoparticles [41–43]. The aggregation of QDs at the Au-caps can be excluded in our case since the SEM pictures do not suggest such behavior.

For a proper discussion of observed PL fluorescence enhancement by Au-caps on SiNWs with respect to our 2D finite element calculations the following statistical considerations can be made. In principle, three cases can be distinguished for the QDs on silicon substrates with statistically distributed straight SiNWs with Au-caps atop: (1) single or (2) agglomerates of several QDs reside somewhere on one of the Au-caps or (3) QDs reside somewhere on the silicon wire or at different positions of the comparably rough Si substrate. For cases (1) and (2), different options are possible: the laser beam can hit and excite the QD such that proper conditions for ideally maximum field enhancement are met, i.e. the PL experiment is carried out and the polarization and direction of the laser beam create an area of field enhancement on the Au-cap (cf the red spot on the Au-cap in figure 7) that coincides with the area where the QD is located or the PL experiment creates a spot of field enhancement but the QDs reside outside this on the Au-cap. In PL mapping experiments (we were mapping several tens of square micrometers) areas of effective PL can be distinguished as 'hot spots'. Following our interpretation of the role of field enhancements for the PL signal of our QDs we can state that these 'hot spots' in the PL are spots where one or more QDs reside on a Au-cap at the right position of field enhancement. In figures 3 and 4 we see PL intensity maps that were taken in 'hot spot' areas in PL mappings. Statistical considerations allow us to state that the PL signal of a single QD or a few QDs on our Si substrate

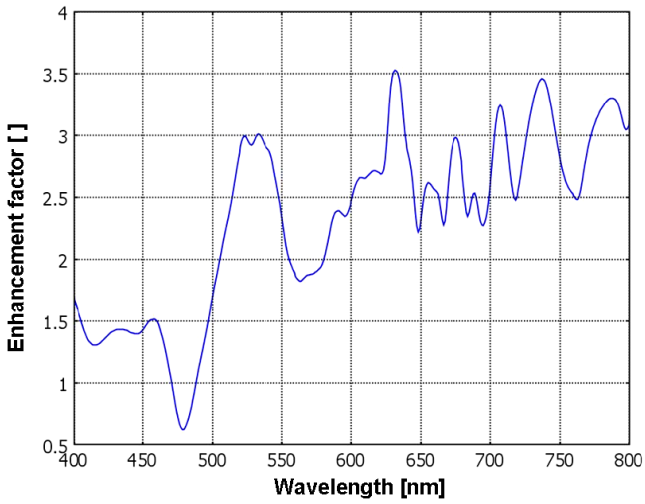

Figure 8. Maximum enhancement factor deduced from 2D FE calculations as shown in figure 6 (for a spherical Au-cap) as a function of wavelength of the incident laser light. Various resonances exist in the rather complex configuration of a SiNW with a spherical Au-cap. One of these resonances resides at 704 nm with an enhancement factor of 3.3.

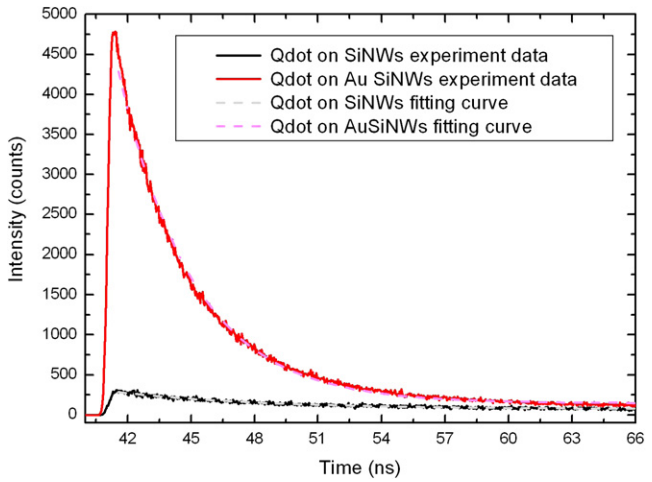

Figure 9. Fluorescence signal analysis of single QDs on SiNWs with and without Au-caps. The time-correlated single photon counting (TCSPC) histogram is shown. By curve fitting, QD lifetimes can be extracted from this measurement, and from the ratio of lifetimes of the QDs on SiNWs with and without Au-caps we can deduce a 2.27-fold fluorescence enhancement due to the field enhancement by the Au-cap.

with SiNWs with Au-caps looks like appearing random and unpredictable. This is essentially due to the fact that the SiNWs with Au-caps show a size and shape distribution and that the 'hot spots' of field enhancement do not spread over the entire Au-cap but are very local, and therefore QDs can sit in 'correct or odd' positions for maximum PL enhancement. However, the principle of using Au-caps to facilitate the PL of single QDs works well as long as enough QDs reside in positions that support PL enhancement. This is not only supported by the measurements in figures 3 and 4 but also by PL mappings (not shown) that show 'hot spots' of PL signals and additionally carried out spontaneous emission experiments of single QDs.

To further strengthen the concept of Au-caps on SiNWs for local field enhancement that can be used to excite the fluorescence of QDs we carried out time-correlated single photon counting (TCSPC) measurements for single QDs sitting on SiNWs with and without Au-caps. The black line in figure 9 shows the accumulated PL intensity for a single QD on a SiNW without a Au-cap, while the red line shows the PL intensity of a single QD on a Au-cap that itself resides on a SiNW. The intensity accumulation was carried out for 60 s with a laser pulse exciting the QDs every 100 ns. After 60 s, there are 6×10^8 excitation cycles, which produce 10^6–10^7 photon counts. This number of counts is enough to obtain sufficiently large statistics. The TCSPC histograms in figure 9 show accumulated photon counts for all cycles. According to the TCSPC histograms, the fluorescence intensities of the single QDs can nicely be fitted by an exponential decay: $I = A_0 + A_1 e^{-t/\tau_1}$, with τ_1 representing the lifetime of a QD, and A_0 and A_1 representing the number of photons (given by counts) that were collected. The accumulated photon counts of all cycles for a single QD on the bare SiNW (see figure 2(c)) is shown in figure 9 (black curve) and the values deduced from this measurement are $A_0 = 55.1$ (counts) and $A_1 = 148.2$ (counts), and the lifetime of the QD is $\tau_1 = 9.78$ ns. For the QD on the Au-capped SiNW (see figure 2(b)) the values deduced from the TCSPC measurements are $A_0 = 106.4$ (counts) and $A_1 = 1779.4$ (counts), and the lifetime of the QD is $\tau_1 = 4.30$ ns. The quantum dot fluorescence enhancement by the Au-cap is characterized by the ratio of lifetimes τ_1. This ratio is also known as a Purcell factor, P [44, 45]. P is proportional to the ratio of spontaneous emission rates, $P \equiv \Gamma_{\text{total}}/\Gamma_0$, while Γ_{total} represents the spontaneous emission rate with field enhancement while Γ_0 represents the spontaneous emission without enhancement, i.e. on the uncoupled single photon emitter. The spontaneous emission rates are inversely proportional to the QD lifetimes of the enhanced and uncoupled QDs and behave according to $P \equiv \Gamma_{\text{total}}/\Gamma_0 \equiv \tau_0/\tau_{\text{total}}$. According to that we got a 2.27-fold enhancement of the QD fluorescence by the Au-caps. The 2.27-fold enhancement is smaller than the 3.6-fold enhancement the calculations suggest. For the excitation wavelength of 400 nm a maximum enhancement of $3.6^2 \times 1.6^2 \sim 33$ (the 1.6 is taken from figure 8) appears to be possible. The discrepancy in enhancement between experiment and simulation can, as mentioned before, be due to a non-optimal location of the QD with respect to the position of maximum field enhancement on the Au-cap. A larger number of experiments and better statistics of this type of TCSPC measurement are currently in preparation. These measurements will hopefully elucidate under which conditions the measured enhancement gets closer to the theoretical maximum value of 33 for the excitation wavelength in use.

5. Conclusion

The preparation of VLS silicon nanowires with Au-caps atop represents a new strategy for the realization of signal-enhancing substrates based on plasmonic effects. These

substrates have proved to be good candidates for ultrasensitive (due to signal enhancement mediated by the Au-nanocaps) detection of fluorescence photoluminescence (PL) signals of highly dilute core/shell CdSeTe/ZnS quantum dots (QDs) in aqueous suspension. The SiNW-based templates may not be the most effective ones for field enhancement due to the Au-cap shapes and sizes. However, these templates are easy to realize on a wafer level, inexpensive, and fast to fabricate, since VLS SiNW growth by chemical vapor deposition is a bottom-up, self-organized process that does not require any top-down nanolithography. Most importantly, this approach is compatible with well-established silicon processing, making on-chip detection devices feasible.

Acknowledgments

J W Chou sincerely thanks C T Yuan, I J Lai, C S Yang, Y L Hung, Y J Lee at the Department of Electrophysics, National Chiao Tung University, Taiwan, and Y T Chong and C T Chiang at the MPI-Microstructure Physics, Halle, Germany for experimental support and valuable discussions. A Bochmann from IPHT carried out the EBSD measurements. This work is supported by the National Science Council, Taiwan, under Grant no. NSC95-2119-M-009-030, by the German Science Foundation, DFG under contract no. CH159/6-1, and by research grants from the state of Saxony Anhalt and the 'nanostress' project funded by the MPG.

References

[1] Efros A L and Efros A L 1982 *Sov. Phys.—Semicond.* **16** 772
[2] Ekimov A I and Onushchenko A A 1982 *Sov. Phys.—Semicond.* **16** 775
[3] Yoffe A D 2001 *Adv. Phys.* **50** 1
[4] Alivisatos A P 1996 *J. Phys. Chem.* **100** 13226
[5] Alivisatos A P 1996 *Science* **271** 933
[6] Bruchez M Jr, Moronne M, Gin P, Weiss S and Alivisatos A P 1998 *Science* **281** 2013
[7] Chan W C W and Nie S 1998 *Science* **281** 2016
[8] Qu L H and Peng X G 2002 *J. Am. Chem. Soc.* **124** 2049
[9] Zhong X H, Feng Y Y, Knoll W and Han M Y 2003 *J. Am. Chem. Soc.* **125** 13559
[10] Bailey R E and Nie S M 2003 *J. Am. Chem. Soc.* **125** 7100
[11] Kim S, Fisher B, Eisler H J and Bawendi M 2003 *J. Am. Chem. Soc.* **125** 11466
[12] Wehrenberg B L, Wang C J and Guyot-Sionnest P 2002 *J. Phys. Chem.* B **106** 10634
[13] Rosenthal S J 2001 *Nat. Biotechnol.* **19** 621
[14] Pollock C 1995 *Fundamentals of Optoelectronics* (Boston, MA: Irwin)
[15] Wu X Y, Liu H J, Liu J Q, Haley K N, Treadway J A, Larson J P, Ge N F, Peale F and Bruchez M P 2003 *Nat. Biotechnol.* **21** 41
[16] Parak W J *et al* 2002 *Chem. Mater.* **14** 2113
[17] Pathak S, Choi S K, Arnheim N and Thompson M E 2001 *J. Am. Chem. Soc.* **123** 4103
[18] Auman E R, Anderson G P, Tran P T, Mattoussi H, Charles P T and Mauro J M 2002 *Anal. Chem.* **74** 841
[19] Willard D M, Carillo L L, Jung J and Van Orden A 2001 *Nano Lett.* **1** 469
[20] Clapp A R, Medintz I L, Mauro J M, Fisher B R, Bawendi M G and Mattoussi H 2004 *J. Am. Chem. Soc.* **126** 301
[21] Auman E R, Clapp A R, Anderson G P, Uyeda H T, Mauro J M, Medintz I L and Mattoussi H 2004 *Anal. Chem.* **76** 684
[22] Lingerfelt B M, Mattoussi H, Auman E R, Mauro J M and Anderson G P 2003 *Anal. Chem.* **75** 4043
[23] Tran P T, Auman E R, Anderson G P, Mauro J M and Mattoussi H 2002 *Phys. Status Solidi* b **229** 427
[24] Willard D M and Van Orden A 2003 *Nat. Mater.* **2** 575
[25] Wagner R S and Ellis W C 1964 *Appl. Phys. Lett.* **4** 89
[26] Givargizov E I 1975 *J. Cryst. Growth* **31** 20
[27] Sivakov V, Andrä G, Gösele U and Christiansen S 2006 *Phys. Status Solidi* a **203** 3692
Sivakov V, Andrä G, Himcinschi C, Gösele U, Zahn D R T and Christiansen S 2006 *Appl. Phys.* A **85** 311
Stelzner Th, Andrä G, Wendler E, Wesch W, Scholz R, Gösele U and Christiansen S H 2006 *Nanotechnology* **17** 2895
Christiansen S H, Singh R, Scholz R, Gösele U, Stelzner Th, Andrä G and Wendler E 2006 *J. Appl. Phys.* **100** 084323
[28] Sivakov V, Heyroth F, Falk F, Andrä G and Christiansen S 2007 *J. Cryst. Growth* **300** 288
[29] Johnson P and Christie R 1972 *Phys. Rev.* B **6** 4370
[30] http://tools.invitrogen.com
[31] Jin J 2002 *The Finite Element Method in Electromagnetics* (New York: Wiley)
[32] Ross F M, Tersoff J and Reuter M C 2005 *Phy. Rev. Lett.* **95** 146104
[33] Hannon J B, Kodambaka S, Ross F M and Tromp R M 2006 *Nature* **440** 69
[34] Gösele U 2006 *Nature* **440** 34
[35] Ostwald W 1900 *Z. Phys. Chem.* **34** 495
Wagner C 1961 *Z. Elektrochem.* **65** 581
Lifschitz I M and Slyozov V V 1981 *Phys. Chem. Solids* **19** 35
[36] Christiansen S, Vogel A, Sivakov V, Bürki G and Michler J 2009 unpublished result
[37] Woodruff J H, Ratchford J B, Goldthorpe I A, McIntyre P C and Chidsey C E D 2007 *Nano Lett.* **7** 1637
[38] Moskovits M 1985 *Rev. Mod. Phys.* **57** 783
[39] Otto A, Mrozek I, Grabhorn H and Akemann W 1992 *J. Phys.: Condens. Matter* **4** 1143
[40] Ehrhold K, Becker M, Gösele U and Christiansen S 2009 unpublished result
[41] Kalele S, Deshpande A C, Bhushan S and Kulkarni S K 2008 *Bull. Mater. Sci.* **31** 541
[42] Zhang J and Lacowicz J R 2006 *J. Phys. Chem.* B **110** 2387
[43] Chen Y, Munechika K, Plante I J-L, Munro A M, Skrabalak S E, Xia Y and Gingera D S 2008 *Appl. Phys. Lett.* **93** 053106
[44] Akimov A V *et al* 2007 *Nature* **450** 402–6
[45] Chang D E, Sørensen A S, Hemmer P R and Lukin M D 2006 *Phys. Rev. Lett.* **97** 053002
[46] Niederberger Ch, Christiansen S H, Lerose D, Sivakov V, Brönstrup G and Michler J 2009 unpublished result